

# Coherent detection schemes for subcarrier wave continuous variable quantum key distribution

E Samsonov<sup>1,2</sup>, R Goncharov<sup>1</sup>, M Fadeev<sup>1</sup>, A Zinoviev<sup>1</sup>,  
D Kirichenko<sup>1</sup>, B Nasedkin<sup>1</sup>, A Kiselev<sup>1</sup>, and V Egorov<sup>1,2,3</sup>

<sup>1</sup> ITMO University, Kronverkskiy, 49, St.Petersburg, 197101, Russia

<sup>2</sup> Quanttelecom LLC., Saint Petersburg, 199178 6 Line 59, Russia

<sup>3</sup> National Center for Quantum Internet, Kronverkskiy, 49, St.Petersburg, 197101, Russia

E-mail: eosamsonov@itmo.ru

**Abstract.** We examine different methods to implement coherent detection in the subcarrier wave quantum key distribution (SCW QKD) systems. For classical wavefields, we present the models describing homodyne-type and heterodyne-type coherent detection schemes needed to extract information from the quadrature phase-coded multimode signals used in SCW QKD. Practical feasibility of the proposed schemes is corroborated by the experiments.

*Keywords:* coherent detection, subcarrier wave, multimode states, quantum communication

Submitted to: *Quantum Sci. Technol.*

## 1. Introduction

Since 1896, when the "beat receptor", the first heterodyne detector, as we know it now, was invented by Nicola Tesla [1], various forms of coherent detection methods, including homodyne and heterodyne detection, have found wide use in a variety of applications. Starting with radio communications [2], the coherent detection methods have been expanded to the optical domain [3]. Nowadays there are numerous examples of optical coherent detection usage in different fields including telecommunications [4, 5, 6, 7, 8] and quantum optics [9, 10, 11]. One of the promising technology at the boundary between these is the quantum key distribution (QKD), which, in combination with coherent detection, leads to a separate branch, known as the continuous variable (CV) QKD [12, 13, 14, 15, 16, 17, 18, 19, 20, 21]. The CV-QKD systems rely on the methods of coherent detection for gaining information encoded in the electromagnetic field quadratures. In other words, single-photon detection can be replaced by conventional optical communication methods.

Active development of novel QKD systems utilising modulated multimode states of light necessitates reconsideration and modification of the existing detection schemes. A striking example of such a system is the subcarrier wave (SCW) QKD [22, 23, 24, 25, 26, 27, 28, 29]. The method for quantum state encoding is the distinguishing feature of the SCW QKD. In this method, a strong monochromatic wave emitted by a laser is modulated in an electro-optic phase modulator to produce weak sidebands, whose relative phase with respect to the strong (carrier) wave encodes the quantum information (a detailed description of the discrete variable (DV) SCW QKD conventional protocol and the SCW CV-QKD protocol can be found in [24] and [29], respectively).

In this paper we present three coherent detection schemes with phase estimation to demodulate the quadrature phase-coded multimode signals. This type of signals is used to encode quantum information in the SCW QKD systems. The main advantage of the proposed schemes is using the carrier wave which plays a leading part in the SCW methodology as a local oscillator (LO). In practice, it provides an alternative solution of the well-known problem of transmitting the local oscillator through the quantum channel (or its generation on the receiver's side). This is the novel approach that has not been previously discussed in works on the multimode CV-QKD [30, 31, 32]. So we present the theoretical models describing the proposed detection schemes and experimentally demonstrate how to implement coherent detection using the carrier wave as a local oscillator.

## 2. Phase-coded multimode signals

Our first step is to describe generation of the phase-coded multimode signals that is the essential part of the SCW QKD system. Since our proof-of-principle experiments use classical light, we shall utilise the classical model of electro-optic phase modulation [33]. Note that quantum description of electro-optic modulation applicable to quantum states can be found in [34, 35, 36].

As is shown in Figure 1, a monochromatic lightwave with the frequency  $\omega$  and the amplitude  $E_0$  is modulated by the traveling wave electro-optic phase modulator using the microwave field with the frequency  $\Omega$  and the phase  $\varphi_a$  [37]. The phase-modulated optical field  $E(t)$  then can be expressed in terms of Jacobi–Anger expansion as follows

$$E(t) = E_0 e^{i\omega t} e^{im_a \cos(\Omega t + \varphi_a)} = E_0 e^{i\omega t} \sum_{k=-\infty}^{\infty} i^k J_k(m_a) e^{ik(\Omega t + \varphi_a)}, \quad (1)$$

where  $J_k(m_a)$  is the  $k$ -order Bessel function of the first kind and  $m_a$  is the modulation index which is typically small in the SCW QKD protocols. As a result, the sidebands are formed at the frequencies  $\omega_k = \omega + k\Omega$ , where  $k$  is the integer.

The modulated light beam emerging at the output of the phase modulator contains the reference carrier ( $k = 0$ ) and the sidebands ( $k \neq 0$ ). The relative phase and amplitude between reference and all the sidebands are determined by the inner microwave field that controls the phase  $\varphi_a$  and the modulation index  $m_a$ , respectively.

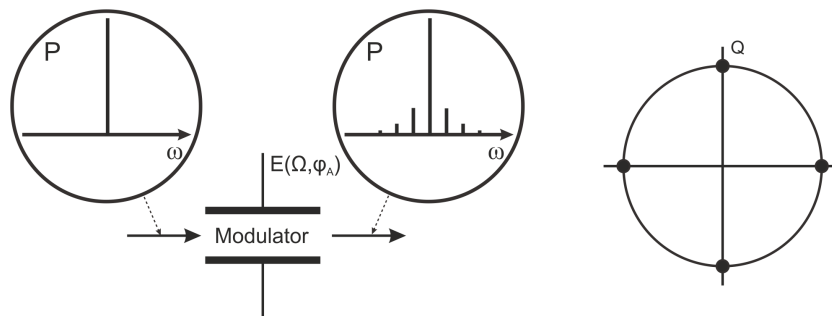


Figure 1: Modulated light emerging after the electro-optic phase modulator and 4-PSK constellation diagram. The typical power spectrum at the modulator output in SCW QKD is also shown.

Therefore one may encode the information into the sidebands of the phase-modulated light by applying different forms of quadrature amplitude modulation [23, 24, 38, 39, 40]. In this paper, for simplicity, we concentrate on the quadrature phase-shift keying which is extensively used in CV-QKDs with discrete modulation [19, 18, 41, 42]. We prepare the phase-coded multimode signals by selecting the phase of the microwave field from the finite set of  $\varphi_a \in \{0, \pi/2, \pi, 3\pi/2\}$  which is equivalent to the four states commonly used in the CV QKD protocols with discrete modulation. An example of the modulated signal constellation diagram is presented in Figure 1.

### 3. Subcarrier wave implementations of coherent detection

#### 3.1. Classical coherent detection

For comparison purposes, we begin with a brief discussion of the basic concepts of coherent detection which is based on using a 50/50 beam splitter to mix an initial weak signal of the power  $P_s$  and the reference field generated by an external source of the power  $P_{LO}$  also known as the local oscillator (LO). The mixed optical fields at the outputs of the beam splitter are detected by a photodiode, and the difference between the signals is registered by a balanced detector. It turned out that the output signal which power is proportional to the square root of LO power,  $\sqrt{P_{LO}}$ , carries the information about the initial signal. In addition, subtraction of the signals results in reduction of noise components, whereas the amplification scheme installed in the balanced detector is used for further amplification of its response.

In the case of homodyne detection, the signal frequency  $\omega_s$  and the LO frequency  $\omega_{LO}$  are equal. The constant signal level that will be observed is determined by the phase difference between the initial signal and the LO,  $\Delta\varphi = \varphi_s - \varphi_{LO}$ . For instance, when the constant signal on the oscilloscope is positive at zero phase difference, it will be negative provided the phase difference equals  $\pi$ . More precisely, in the absence of noise, the output of the detector is proportional to the difference between the photocurrents registered by the photodiodes and, in the absence of noise, can be written in the following

form [6]:

$$I(t) = I_1(t) - I_2(t) = 2R(\lambda)G\sqrt{P_s(t)P_{LO}} \cos \Delta\varphi = 2R(\lambda)GCE_s(t)E_{LO} \cos \Delta\varphi, \quad (2)$$

where  $R(\lambda)$  is the responsivity of photodiodes;  $G$  is the electronic gain of balanced detector;  $C = S/(2\xi)$  is the ratio of the effective beam area  $S$  and the doubled impedance  $\xi$  of the medium;  $E_s$  and  $E_{LO}$  are the amplitudes of the initial signal field and the LO, respectively.

In the case of heterodyning with  $\omega_s \neq \omega_{LO}$ , the intensities of the mix of two harmonic signals contain harmonics oscillating at the difference and the sum frequencies:  $\omega_- = \omega_s - \omega_{LO}$  and  $\omega_+ = \omega_s + \omega_{LO}$ . Since both the optical and the sum frequencies are much larger than the bandwidth of any existing photodiode, the photodetectors are unable to register these high frequency harmonics. Therefore, the output of the balanced detector will be the electrical signal of the difference frequency  $\omega_-$  that stores the information about the phase of the initial signal [43, 44]. This approach allows detecting two quadrature components at the once, since the receiver now does not need to set any phase of the local oscillator. The output photocurrent is given by

$$I(t) = 2R(\lambda)G\sqrt{P_s(t)P_{LO}} \cos(\omega_-t + \Delta\varphi). \quad (3)$$

### 3.2. Coherent detection with single quadrature selection

In this section we describe the coherent detection scheme with single quadrature selection for the SCW QKD system. We keep the Alice's block identical to the original sender block of the system [24] and change the block of Bob by replacing the single photon detector with the balanced detector. Figure 2 details the changes and the mode of operation of the proposed scheme.

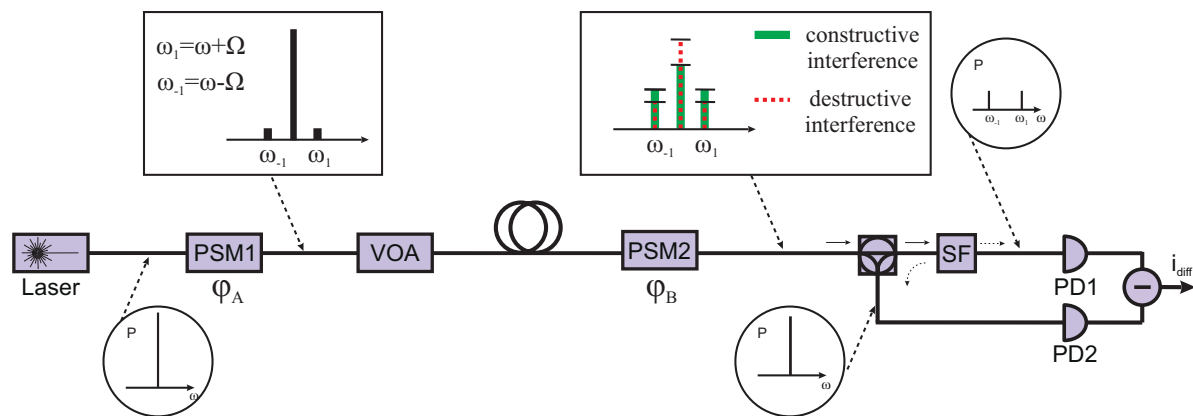


Figure 2: Principal scheme of SCW CV-QKD setup. PSM is the electro-optic phase modulator; VOA is the variable optical attenuator; SF is the spectral filter that cuts off the carrier; PD is the photodiode. Diagrams in circles show the simplified power spectrum, diagrams in squares illustrate the spectrum for various phase shifts. Horizontal dashes mark the levels of intensities and are added for illustrative purposes.

Coherent detection illustrated in Fig. 2 is functionally similar to conventional homodyne detection described in the previous section. By contrast to the homodyne detection scheme, the phase modulator in the Bob's module plays the role of the 50/50 beam splitter. After the second modulation the interference is observed at frequencies  $\omega_k = \omega + k\Omega$  provided that Alice and Bob use the microwave modulating field with identical frequencies.

In other words, the local oscillator is not used directly as a separate source. SCW homodyning occurs as a result of redistribution of the energy between the intense carrier mode and the weak sidebands, as if a strong coherent beam is mixed with them at a beam splitter.

As is illustrated in Fig. 3a (3b), the power of subcarrier wave is higher (lower) than the carrier wave power when the interference is constructive (destructive). A narrow spectral filter then separates the carrier from the sidebands. Finally, the outputs (the carrier and the sidebands) are detected by two different photodiodes, and their photocurrents are subtracted. Thus, one can extract information encoded in the oscillating signal phase. Similar to the conventional homodyne detection in QKD, Bob measures only one quadrature component at a time by selecting the phase of the microwave field from the set of  $\varphi_b \in \{0, \pi/2\}$ .

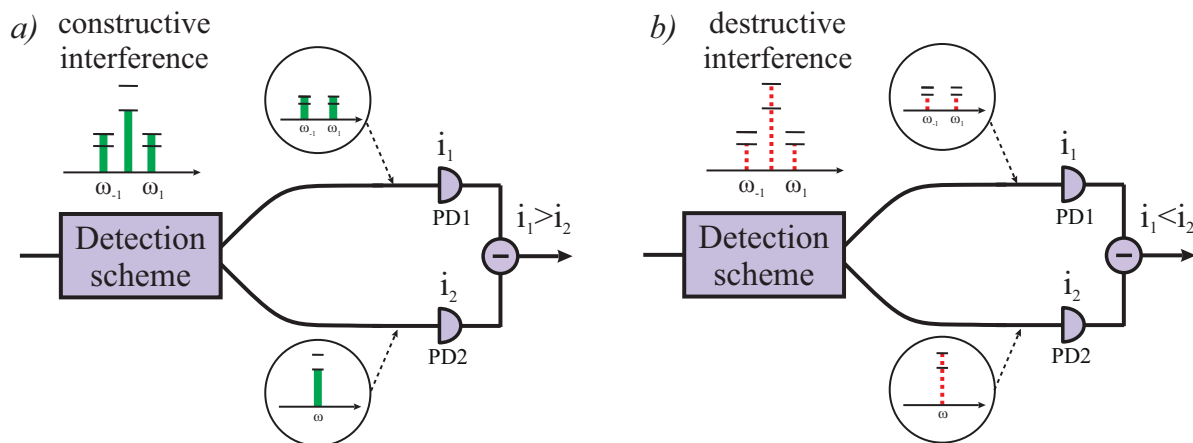


Figure 3: SCW coherent detection scheme. The charts show the energy distribution between the carrier and the subcarriers for (a) constructive and (b) destructive interference.

Now we describe a simple classical model (quantum considerations can be found in [29]) of the above homodyne-like coherent detection scheme. The traveling wave phase modulator on the Bob's side generally differs from the Alice's modulator both in the modulation index,  $m_b \neq m_a$ , and in the phase,  $\varphi_b \neq \varphi_a$ , thus introducing the phase difference  $\Delta\varphi = \varphi_a - \varphi_b$ . The expression for the output field emerging after the second modulator  $E'(t)$

$$E'(t) = E_0 e^{i\omega t} e^{im_a \cos(\Omega t + \varphi_a)} e^{im_b \cos(\Omega t + \varphi_b)} \quad (4)$$

can be simplified with the help of identities

$$m_a \cos(\Omega t + \varphi_a) + m_b \cos(\Omega t + \varphi_b) = m \cos(\Omega t + \phi), \quad (5a)$$

$$m = \sqrt{m_a^2 + m_b^2 + 2m_a m_b \cos(\varphi_a - \varphi_b)}, \quad (5b)$$

$$m e^{i\phi} = m_a e^{i\varphi_a} + m_b e^{i\varphi_b}. \quad (5c)$$

Similar to Eq. (1), the output field can now be written in the form of the Jacobi-Anger expansion:

$$E'(t) = E_0 e^{i\omega t} \sum_{k=-\infty}^{\infty} i^k J_k(m) e^{ik\phi} e^{ik\Omega t} \equiv \sum_{k=-\infty}^{\infty} E_k e^{ik\Omega t}, \quad E_k = E_0 e^{i\omega t} i^{|k|} J_{|k|}(m) e^{ik\phi}. \quad (6)$$

The carrier wave is separated from the sidebands using spectral filtering in the Bob's module. For simplicity, we shall neglect the losses and imperfection of the spectral filter. So, we can single out the component at the central frequency to obtain the following expressions for the fields in two arms of the detector:

$$E_1(t) = E_0 e^{i\omega t} J_0(m), \quad E_2(t) = \sum_{\substack{k=-\infty \\ k \neq 0}}^{\infty} E_k e^{ik\Omega t}. \quad (7)$$

Now we can closely follow the line of reasoning led to Eq. (2), and obtain the time averaged difference of the photocurrents in the form:

$$I = R(\lambda)GC \langle |E_2(t)|^2 - |E_1(t)|^2 \rangle_t = R(\lambda)GC E_0^2 (1 - 2J_0^2(m)), \quad (8)$$

where  $\langle \dots \rangle_t = \tau^{-1} \int_0^\tau \dots dt$ ,  $\tau = 2\pi/\Omega$ . Using temporal averaging assumes that the detectors are insensitive to harmonics of intensities  $|E_1(t)|^2$  and  $|E_2(t)|^2$  oscillating at radio frequencies. Note that modulation keeps the amplitude of the phase-modulated wave (4) unchanged with  $|E'(t)|^2 = E_0^2$ , so that Eq. (6) leads to the unitarity condition  $\sum_{k=-\infty}^{\infty} J_k^2(m) = 1$  used in derivation of the right-hand side of formula (8).

When the phase difference  $\Delta\varphi = \varphi_a - \varphi_b$  is changed, the modulation index  $m$  varies between its minimal value  $m_{\min} = |m_b - m_a|$  at  $\cos(\varphi_a - \varphi_b) = -1$  to the maximal index of modulation  $m_{\max} = m_b + m_a$  at  $\cos(\varphi_a - \varphi_b) = 1$ . In the case where Alice sends non-modulated wave with  $m_a = 0$ , the output voltage (8) will be zero provided the Bob's index of modulation is adjusted to meet the condition:  $J_0(m_b) = 1/\sqrt{2}$ .

Figure 4 shows the curves representing dependence of the output voltage on the phase shift  $\varphi_a$  for the in-phase component  $I$  and the quadrature component  $Q$  that are computed at  $\varphi_b = 0$  and  $\varphi_b = \pi/2$ , respectively. In our calculations, the parameters are taken to be close to those used in the experiments verifying our model. These are: the carrier wave power is  $P_c = 10 \mu\text{W}$ ; the modulation index of Alice is  $m_a = 0.09$ ; the responsivity of the photodiodes is  $R = 0.6$ ; and the additional gain of the detectors is  $G = 4 \times 10^3$ .

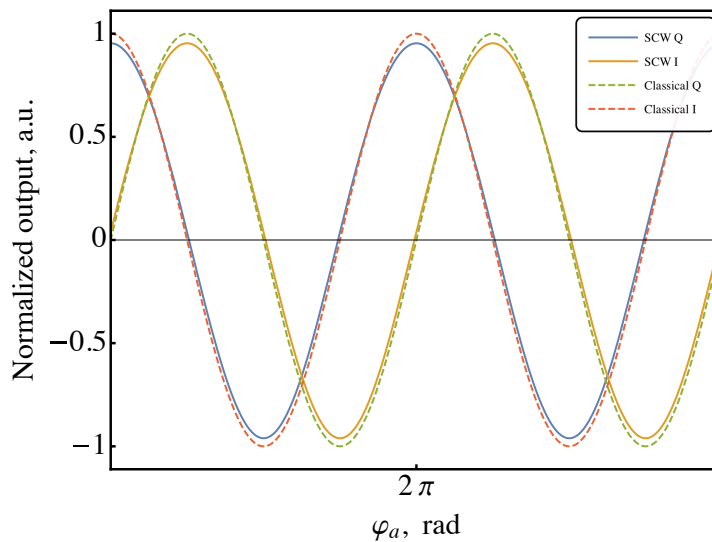


Figure 4: The in-phase and the quadrature components of the normalized output signals from the SCW coherent detection scheme (see Eq. (9)) and the classical homodyne scheme.

In order to draw analogy between the proposed scheme and conventional homodyne detection, we assume that the temporally averaged intensities  $\langle |E_1(t)|^2 \rangle_t$  and  $\langle |E_2(t)|^2 \rangle_t$  of the carrier and the subcarrier waves at the output of Alice's modulator correspond to the intensities of the signal and reference waves:  $E_s = E_0 \sqrt{1 - J_0^2(m_a)}$  and  $E_{LO} = E_0 J_0(m_a)$ . Then, for the classical homodyne scheme, the curves for the normalized output voltage (2)  $I/I_{\max} = \cos(\Delta\varphi)$  are plotted in Figure 4. It can be seen that the normalized output signal (8) for our scheme

$$I/I_{\max} = \frac{1 - 2J_0^2(m)}{2J_0(m_a)\sqrt{1 - J_0^2(m_a)}} \quad (9)$$

agrees closely with the predictions of the classical homodyne scheme.

### 3.3. Simultaneous selection of both quadrature component

An important point is that it is possible to construct an optical phase-diversity coherent detection scheme. In this scheme, the receiver is similar to 90° optical hybrid and both the quadrature components can be measured simultaneously. The principal scheme of SCW CV-QKD setup utilizing such a receiver is shown in Figure 5. In this setup, the Y beam splitter is combined with the two coherent detection schemes where the electro-optic phase modulators are displaced in phase by 90°.

By using the detection scheme depicted in Figure 5, we can measure the two output signals,  $E_{1I}(t)$  and  $E_{2I}(t)$ , from the top arm of the detector with the phase  $\varphi_b = 0$ , whereas the output signals,  $E_{1Q}(t)$  and  $E_{2Q}(t)$ , from the bottom arm emerge from the detector with the phase  $\varphi_b = \pi/2$ . Then the output currents after the balanced detectors are converted to the voltages  $V_{I,Q}$ . Hence by using these two balanced detectors we

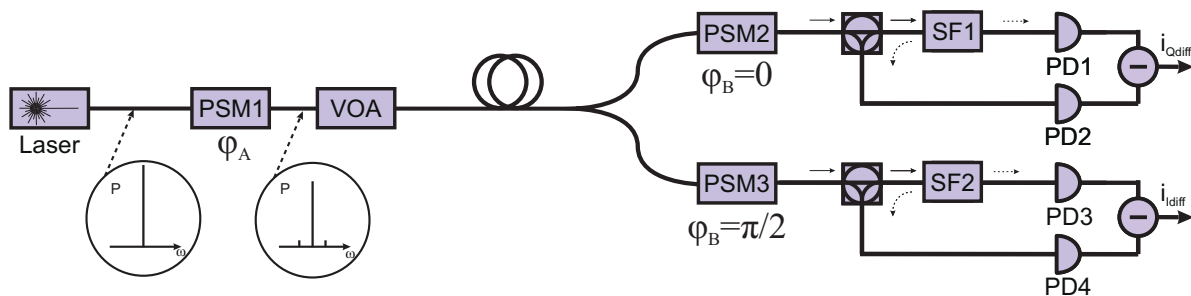


Figure 5: Principal scheme of SCW CV-QKD setup with phase-diversity coherent receiver.

can perform simultaneous I/Q measurements. Note, however, that this approach will introduce an additional 3 dB loss at the detection stage and its QKD security should be carefully analyzed.

### 3.4. Heterodyne detection

Another well-known method to obtain information about the optical complex amplitude is heterodyne detection [3, 6, 45, 46, 47, 48]. In this section we show how a heterodyne-type detection scheme can be adopted for quadrature phase-coded multimode signals. The mode of operation of our coherent detection scheme demonstrating versatility of the SCW method is described in Figure 6. Note also that such scheme promises significant simplification of implementation.

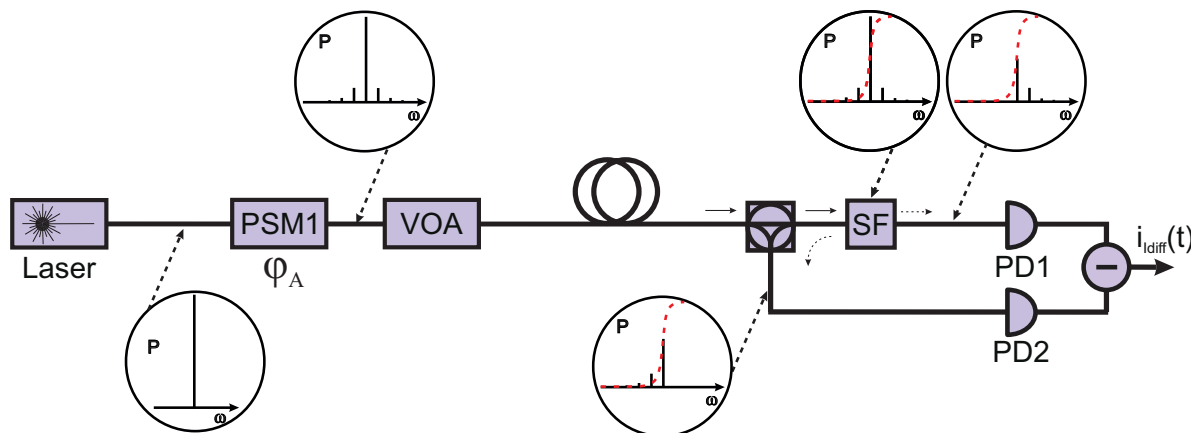


Figure 6: Principal scheme of SCW CV-QKD setup with heterodyne detection. Examples of power spectra are shown in encircled diagrams and  $i_{\text{diff}}$  stands for the output photocurrent.

As is shown in Figure 6, similar to the scheme presented in Figure 2, the only component changed in the initial system [24, 25] is the Bob's block whose detection scheme is no longer using the phase modulator. In this scheme spectral filtering is used to mix the carrier wave with the upper and the lower sidebands where subcarrier



frequencies are higher and below the carrier frequency  $\omega$ . For this purpose, the spectral filter bandpass is chosen so as to pass light at the frequency  $\omega + \Omega$  and to halve the intensity of the carrier at the frequency  $\omega$ , whereas the rest of light is reflected back. In other words, the transparency of the spectral filter,  $T$ , should meet the conditions:  $T(\omega) \approx 0.5$ ,  $T(\omega - \Omega) \rightarrow 0$  and  $T(\omega + \Omega) \rightarrow 1$ .

From Eq. (1) we obtain the fields in the separate arms in the following form:

$$E_1(t) = E_0 e^{i\omega t} \left( \sum_{k=1}^{\infty} i^k J_k(m_a) e^{ik(\Omega t + \varphi_a)} + \sqrt{0.5} J_0(m_a) \right), \quad (10)$$

$$E_2(t) = E_0 e^{i\omega t} \left( \sum_{k=1}^{\infty} i^k J_k(m_a) e^{-ik(\Omega t + \varphi_a)} + \sqrt{0.5} J_0(m_a) \right), \quad (11)$$

where we have used the identity  $J_{-\alpha}(x) = (-1)^\alpha J_\alpha(x)$  for the Bessel functions. When the modulation index  $m_a$  is small, we can apply the lowest order approximation that takes into account only the first order subcarriers

$$E_1(t) \approx E_0 (iJ_1(m_a) e^{i(\omega + \Omega)t + \varphi_a} + \sqrt{0.5} J_0(m_a) e^{i\omega t}), \quad (12)$$

$$E_2(t) \approx E_0 (iJ_1(m_a) e^{i(\omega - \Omega)t - \varphi_a} + \sqrt{0.5} J_0(m_a) e^{i\omega t}), \quad (13)$$

where  $\omega_\pm = \omega \pm \Omega$ , and derive the output photocurrent in the absence of noise

$$I(t) = R(\lambda)GC(|E_2(t)|^2 - |E_1(t)|^2) = R(\lambda)GC2\sqrt{2}E_0^2 J_0(m_a) J_1(m_a) \sin(\Omega t + \varphi_a). \quad (14)$$

Clearly, this result bears a striking resemblance to the classical heterodyning.

As in the previous section, we now discuss this analogy using Eq. (3) with  $\omega$  and  $\Delta\varphi$  replaced by  $\Omega$  and  $\varphi_a + \pi/2$ , respectively. For this purpose, we assume that the amplitudes of the signal and reference waves are  $E_s = E_0 \sqrt{1 - J_0^2(m_a)}$  and  $E_{LO} = E_0 J_0(m_a)$  and compare the output of the classical heterodyne,  $I_{\max} \sin(\Omega t + \varphi_a)$ , with the signal given in Eq. (14). Figure 7 shows that the normalized output of our scheme

$$I(t)/I_{\max} = \frac{\sqrt{2}J_1(m_a)}{\sqrt{1 - J_0^2(m_a)}} \sin(\Omega t + \varphi_a) \quad (15)$$

turns out to be very close to the output of the classical scheme. It should be stressed that, in this analysis, the detectors are assumed to be sensitive to the radio frequency  $\Omega$ .

Demodulation of the received signal can be carried out by standard telecommunication methods using a quadrature synchronous demodulator [6, 49, 50, 51, 52]. The demodulator setup allows one to observe the in-phase (initial) and quadrature (shifted by  $\pi/2$  using a voltage generator) signal components simultaneously on the analyzer and thus extract the information on the phase selected by Alice.

The main disadvantage of this method is emerging conflict between spectral filtering and bandwidth of balanced detector. On the one hand, an increase of modulation

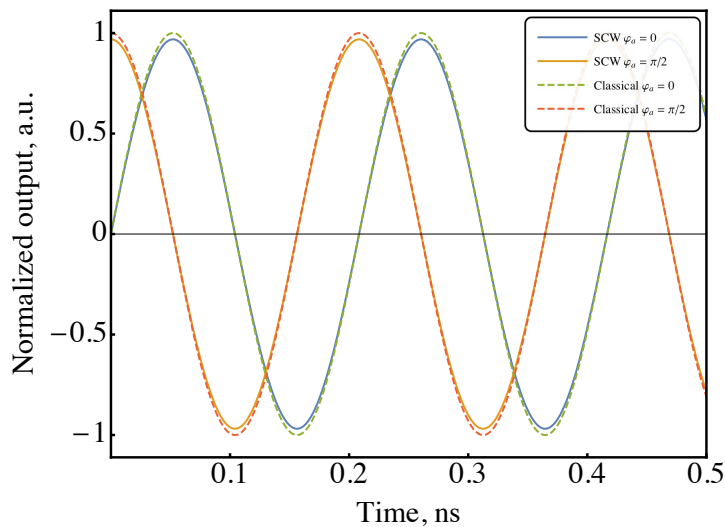


Figure 7: Time dependence of the normalized heterodyne-derived signals for the SCW and the classical detection schemes.

frequency  $\Omega$  leads to the growth of required detector's bandwidth, what results in extra electronic noises [53]. Usually bandwidth of balanced detectors used for quantum measurements is less than 1 GHz [54]. On the other hand, low modulation frequencies perplex subcarriers' spectral filtering. Thus one of the main challenges for practical implementation of such scheme is to find an optimal modulation frequency that satisfies both of these conditions.

#### 4. Experimental results

In this section we present the results of our experiments verifying the theoretical models presented in the previous section. For the homodyne-like detection setup shown in Figure 2, our proof-of-principle experiment have used a 1550 nm 10  $\mu\text{W}$  fiber-coupled laser directed into the LiNbO<sub>3</sub> electro-optic phase modulator with the electrical signal frequency  $\Omega = 4.8$  GHz. The modulation index  $m_b$  is adjusted to maximize the difference between the results for different values of  $\Delta\varphi$  and the phase dependence of the output voltage is expected to be nearly harmonic (see Figure 4). After the second modulation the spectral components are transmitted through the circulator to a fiber Bragg grating spectral filter. The two output ports of the circulator are coupled to the input ports of a self-developed balanced detector (the measurement bandwidth is 100 MHz, the gain is  $G = 4 \cdot 10^3$  and the responsivity is  $R = 0.6$ ).

Figure 8 presents the output voltage measured in relation of time when the phase difference (the phase  $\varphi_a$  is set to be zero),  $\Delta\varphi$ , undergoes time-periodic piecewise changes between the states with equidistant values from a discrete set  $\{0, \pi/2, \pi, 3\pi/2\}$ . Referring to Fig. 8a, it can be seen that, in the case where the carrier wave power after the modulation was  $P_c = 9.96 \mu\text{W}$  and the total power of the subcarriers was  $P_s = 40.00 \text{ nW}$ , variations of the voltage level are almost indiscernible. By contrast,

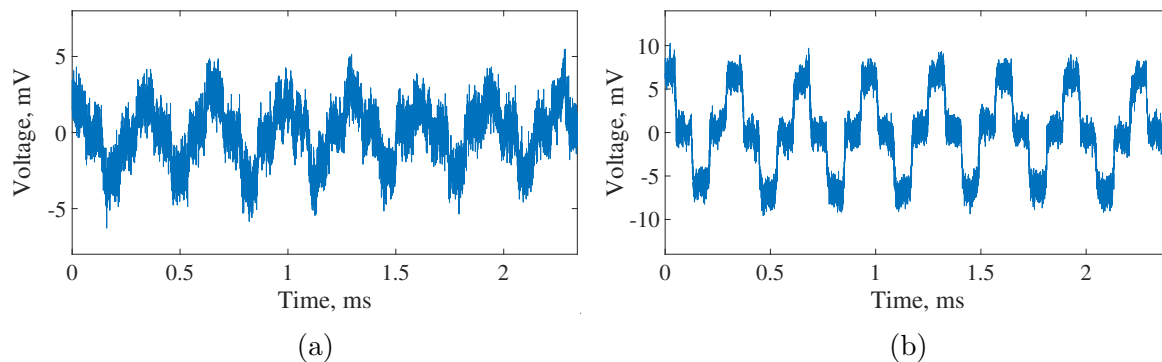


Figure 8: Time dependence of the output voltage for the homodyne-like coherent detection scheme shown in Fig. 2. The extreme points correspond to the constructive and destructive interference. The phase difference  $\Delta\varphi$  varies periodically in time switching between the values from a discrete set:  $\{0, \pi/2, \pi, 3\pi/2\}$ . Two cases are shown: (a)  $P_c = 9.96 \mu\text{W}$ ,  $P_s = 40.00 \text{ nW}$ ; and (b)  $P_c = 9.5 \mu\text{W}$ ,  $P_s = 500.00 \text{ nW}$ .

Figure 8b demonstrates the case with unambiguously distinguishable voltage levels that occurs at  $P_c = 9.5 \mu\text{W}$  and  $P_s = 500.00 \text{ nW}$ . Thus, our coherent detection scheme is sufficiently sensitive to estimate the phase of the quadrature phase-coded multimode signals from the electro-optic phase modulator.

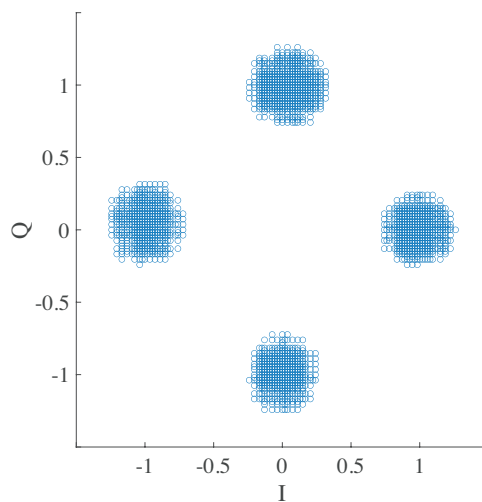


Figure 9: 4-PSK constellation diagram recovered from the phase-modulated optical signal,  $P_c = 9.5 \mu\text{W}$ ,  $P_s = 500.00 \text{ nW}$ .

We have also performed the experiment for the optical phase-diversity coherent receiver sketched in Figure 5. The 4-PSK constellation diagram recovered from the phase-modulated optical signal using the optical phase-diversity coherent receiver is depicted in Figure 9.

In order to test the heterodyne scheme (see Figure 6), we need to get around the

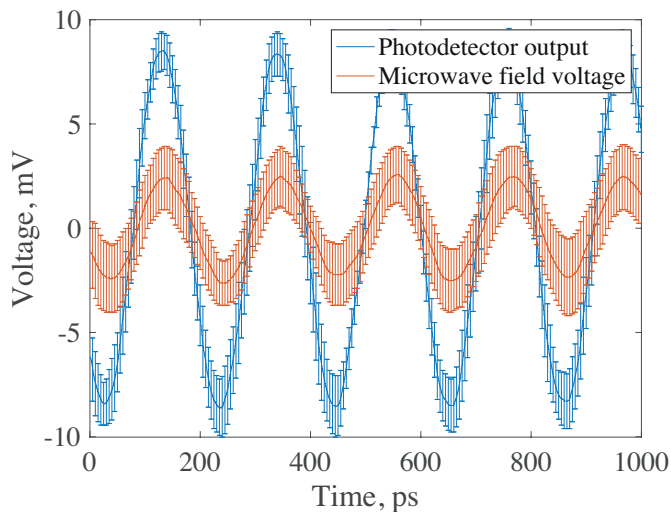


Figure 10: Time dependence of microwave field voltage and the output voltage for balanced detector's single arm ( $P_c = 225.00 \mu\text{W}$ ,  $P_s = 146.50 \mu\text{W}$ ) using the SCW heterodyning. Mean values are indicated along with standard deviations.

above-mentioned difficulties concerning the frequency bandwidth. For this purpose, we have utilized the photodetector with 6.17 GHz bandwidth in the single arm of the scheme described in Figure 6 to obtain the signal at the intermediate frequency. The measured curves for the output voltage and the microwave field are presented in Figure 10. The results show that the signal light is down-converted to the intermediate frequency coincident with the frequency of the microwave field used in the electro-optic phase modulator.

## 5. Conclusion

In this paper we have applied several approaches to put coherent detection schemes into the framework of the subcarrier wave QKD systems. In our homodyne-like coherent detection schemes (see Sec. 3.2 and Sec. 3.3), the phase-modulated light emerging from the Bob's modulator is splitted into the carrier and the subcarrier waves and the output signal is determined by the difference between the responses of the photodiodes to the light of these two waves. By contrast, in our heterodyne-type detection scheme described in Sec. 3.4 the light modulated by Alice is directly used as the input wave. This wave, similar to the homodyne-like scheme, is divided into two waves. But, in contrast to this scheme, these waves are obtained by filtering out either the lower or the upper sidebands. In this case, we have shown that the differential signal which is oscillating with the microwave frequency can be used to extract the information about the phase encoded by Alice.

In our theoretical considerations we have presented simple classical models emphasizing the analogy between the suggested coherent detection schemes and the

standard homodyne/heterodyne methods. Our experimental results clearly demonstrate practical feasibility of the detection schemes. Further development will require a more sophisticated and detailed analysis of these schemes using the methods of quantum optics. This will allow their legitimate employment in quantum computing, quantum cryptography, and quantum tomography.

## Acknowledgments

This work was funded by Government of Russian Federation (Grant No. MK-777.2020.8).

## References

- [1] Anderson L I 1994 *Nicola Tesla: Lecture Before the New York Academy of Sciences - April 6, 1897* (Twenty First Century Books)
- [2] Roger B and Georges H 1952 Double heterodyne radio receiver US Patent 2,606,285
- [3] Protopopov V V 2009 *Laser Heterodyning* (Springer Berlin Heidelberg)
- [4] Ly-Gagnon D S, Tsukamoto S, Katoh K and Kikuchi K 2006 *Journal of lightwave technology* **24** 12
- [5] Tanosaki S, Sasaki Y, Takagi M, Ishikawa A, Inage H, Emori R, Suzuki J, Yuasa T, Taniguchi H, Devaraj B *et al.* 2003 *Optical review* **10** 447–451
- [6] Kikuchi K 2015 *Journal of Lightwave Technology* **34** 157–179
- [7] Mecozzi A and Shtaif M 2018 *Optics express* **26** 33970–33981
- [8] Lu Y, Zhu T, Chen L and Bao X 2010 *Journal of lightwave Technology* **28** 3243–3249
- [9] Yuen H P and Chan V W 1983 *Optics letters* **8** 177–179
- [10] Barchielli A 1990 *Quantum Optics: Journal of the European Optical Society Part B* **2** 423
- [11] Wallentowitz S and Vogel W 1996 *Physical Review A* **53** 4528
- [12] Grosshans F, Van Assche G, Wenger J, Brouri R, Cerf N J and Grangier P 2003 *Nature* **421** 238–241
- [13] Hirano T, Yamanaka H, Ashikaga M, Konishi T and Namiki R 2003 *Physical Review A* **68** 042331
- [14] Leverrier A and Grangier P 2011 *Physical Review A* **83** 042312
- [15] Heid M and Lütkenhaus N 2006 *Physical Review A* **73** 052316
- [16] Brádler K and Weedbrook C 2018 *Physical Review A* **97** 022310
- [17] Papanastasiou P, Lupo C, Weedbrook C and Pirandola S 2018 *Physical Review A* **98** 012340
- [18] Ghorai S, Grangier P, Diamanti E and Leverrier A 2019 *Physical Review X* **9** 021059
- [19] Lin J, Upadhyaya T and Lütkenhaus N 2019 *Physical Review X* **9** 041064
- [20] Zhang G, Haw J, Cai H, Xu F, Assad S, Fitzsimons J, Zhou X, Zhang Y, Yu S, Wu J *et al.* 2019 *Nature Photonics* **13** 839–842
- [21] Zhang Y, Chen Z, Pirandola S, Wang X, Zhou C, Chu B, Zhao Y, Xu B, Yu S and Guo H 2020 *Phys. Rev. Lett.* **125**(1) 010502
- [22] Merolla J M, Mazurenko Y, Goedgebuer J P, Porte H and Rhodes W T 1999 *Optics letters* **24** 104–106
- [23] Mora J, Ruiz-Alba A, Amaya W, Martínez A, García-Muñoz V, Calvo D and Capmany J 2012 *Optics letters* **37** 2031–2033
- [24] Gleim A, Egorov V, Nazarov Y V, Smirnov S, Chistyakov V, Bannik O, Anisimov A, Kynev S, Ivanova A, Collins R *et al.* 2016 *Optics express* **24** 2619–2633
- [25] Miroshnichenko G, Kozubov A, Gaidash A, Gleim A and Horoshko D 2018 *Optics express* **26** 11292–11308
- [26] Gaidash A, Kozubov A and Miroshnichenko G 2019 *JOSA B* **36** B16–B19

- [27] Chistiakov V, Kozubov A, Gaidash A, Gleim A and Miroshnichenko G 2019 *Optics Express* **27** 36551–36561
- [28] Kynev S M, Chistyakov V V, Smirnov S V, Volkova K P, Egorov V I and Gleim A V 2017 *Journal of Physics: Conference Series* **917** 052003
- [29] Samsonov E, Goncharov R, Gaidash A, Kozubov A, Egorov V and Gleim A 2020 *Scientific Reports* **10** 10034
- [30] Fang J, Huang P and Zeng G 2014 *Physical Review A* **89** 022315
- [31] Gyongyosi L and Imre S 2019 *Journal of Statistical Physics* **177** 960–983
- [32] Wang Y, Mao Y, Huang W, Huang D and Guo Y 2019 *Optics express* **27** 25314–25329
- [33] Haykin S 2008 *Communication systems* (John Wiley & Sons)
- [34] Miroshnichenko G P, Kiselev A D, Trifanov A I and Gleim A V 2017 *JOSA B* **34** 1177–1190
- [35] Capmany J and Fernández-Pousa C R 2010 *JOSA B* **27** A119–A129
- [36] Kumar P and Prabhakar A 2008 *IEEE journal of quantum electronics* **45** 149–156
- [37] Yariv A and Yeh P 1984 *Optical waves in crystals* vol 5 (Wiley New York)
- [38] Gonzalez N G, Zibar D, Yu X and Monroy I T 2010 Optical phase-modulated radio-over-fiber links with k-means algorithm for digital demodulation of 8psk subcarrier multiplexed signals *Optical Fiber Communication Conference* (Optical Society of America) p OML3
- [39] Gasulla I and Capmany J 2012 *Optics express* **20** 11710–11717
- [40] Zhang Y, Xu K, Zhu R, Li J, Wu J, Hong X and Lin J 2008 *Optics letters* **33** 2332–2334
- [41] Hirano T, Ichikawa T, Matsubara T, Ono M, Oguri Y, Namiki R, Kasai K, Matsumoto R and Tsurumaru T 2017 *Quantum Science and Technology* **2** 024010
- [42] Leverrier A 2009 *Theoretical study of continuous-variable quantum key distribution* Ph.D. thesis Télécom ParisTech
- [43] Yoshida M, Goto H, Kasai K and Nakazawa M 2008 *Optics Express* **16** 829–840
- [44] Hongo J, Kasai K, Yoshida M and Nakazawa M 2007 *IEEE Photonics Technology Letters* **19** 638–640
- [45] Gebbie H, Stone N, Putley E and Shaw N 1967 *Nature* **214** 165–166
- [46] Maznev A, Nelson K and Rogers J A 1998 *Optics letters* **23** 1319–1321
- [47] Fried D L 1967 *Proceedings of the IEEE* **55** 57–77
- [48] DeLange O 1968 *IEEE spectrum* **5** 77–85
- [49] Bylina M, Glagolev S and Diubov A 2017 *Proceedings of Telecommunication Universities* **3** 21–28
- [50] Wang C, Qu Y and Tang Y P T 2015 *Infrared Physics & Technology* **72** 191–194
- [51] Bohme R and Eichin M 1999 Heterodyne receiver with synchronous demodulation for receiving time signals US Patent 5,930,697
- [52] Chen Y K, Koc U V and Leven A 2010 Optical heterodyne receiver and method of extracting data from a phase-modulated input optical signal US Patent 7,650,084
- [53] Chi Y M, Qi B, Zhu W, Qian L, Lo H K, Youn S H, Lvovsky A and Tian L 2011 *New Journal of Physics* **13** 013003
- [54] Tang X, Kumar R, Ren S, Wonfor A, Penty R and White I 2020 *Optics Communications* 126034